




# Synthesis of Pd/conjugated microporous polymer heterogeneous catalysts via imine groups and high catalytic efficiency on Suzuki–Miyaura coupling reaction

Yu Zang<sup>1,2,\*</sup> , Shan Gao<sup>1</sup>, Boyu Jing<sup>1</sup>, Hong Sun<sup>1</sup>, Jianjun Wang<sup>1</sup>, Jiao Liu<sup>1</sup>, Fengjuan Miao<sup>3</sup>, and Liang Xu<sup>4,\*</sup>

<sup>1</sup> College of Materials Science and Engineering, Qiqihar University, Wenhua Street 42, Qiqihar 161006, Heilongjiang, China

<sup>2</sup> Jiangsu Engineering Laboratory of Novel Functional Polymeric Materials, Soochow University, Suzhou 215123, China

<sup>3</sup> College of Communications and Electronics Engineering, Qiqihar University, Wenhua Street 42, Qiqihar 161006, Heilongjiang, China

<sup>4</sup> Analysis and Testing Center, Qiqihar University, Wenhua Street 42, Qiqihar 161006, Heilongjiang, China

**Received:** 2 November 2022

**Accepted:** 28 November 2022

**Published online:**

14 December 2022

© The Author(s), under exclusive licence to Springer Science+Business Media, LLC, part of Springer Nature 2022

## ABSTRACT

Four kinds of conjugated microporous polymers (CMPs) with imine structures were synthesized by a Sonogashira coupling reaction followed by a postreaction between aldehydes and amines. Palladium nanoparticles (Pd NPs) were successfully supported on the CMPs to prepare Pd/CMP heterogeneous catalysts and were used to catalyze the Suzuki–Miyaura coupling reaction. The number of aromatic nuclei and nitrogen atoms in the CMPs highly affects Pd loading. In the Suzuki–Miyaura coupling reaction, the Pd/CMP with good Pd NPs dispersibility and appropriate Pd content (Pd/CMP-NA) exhibited the highest catalytic efficiency with 100% conversion and 95.4% yield which can be used for many substrates. The Pd/CMP-NA heterogeneous catalyst was easy to recover and still exhibited good catalytic efficiency after 5 cycles. To further understand the catalytic mechanism of Pd/CMP-NA on the Suzuki–Miyaura coupling reaction, we proposed a rational catalytic cycle. This paper provides an idea for the structural design of CMPs used for Suzuki–Miyaura catalytic reaction.

Handling Editor: Maude Jimenez.

Address correspondence to E-mail: zangyu.25@163.com; m13069984921@163.com

## Introduction

The Suzuki–Miyaura coupling reaction refers to the cross-coupling reaction of aryl or alkenyl boronic acid with halogenated aromatic hydrocarbons or alkenes under the catalysis of zero-valent Pd [1]. This reaction was published in 1979 by Akira Suzuki, a 2011 Nobel Prize winner, and is widely used to synthesize many natural products and organic materials, such as polyolefins, styrene and biphenyl derivatives, and exhibits strong substrate applicability [2–7]. Homogeneous palladium catalysts have been widely studied by many scholars due to their excellent catalytic performance, but they are expensive and difficult to separate and reuse. At the same time, Pd species may also cause pollution that is toxic to products, and their practical application is largely limited [8–10]. In contrast, heterogeneous catalysts can be recycled through simple separation methods, overcoming the shortcomings of homogeneous catalysis [11–15]. In recent years, palladium nanoparticles (Pd NPs) with small diameters (1–10 nm) have become the focus of catalysis research because they exhibit high catalytic efficiency in various organic solvents because of their high surface to volume ratio and quantum size effect. However, these Pd NPs are unstable due to their high surface energy and are prone to form Pd agglomerates, resulting in reduced activity or even deactivation, which limits their wide application [16–20]. Therefore, finding suitable support materials is a great challenge in the field of heterogeneous catalysis. Various materials, such as mesoporous silica, zeolites, and porous organic polymers (POPs), have been successfully used as heterogeneous catalytic carriers so far [21–25]. Among these supports, POPs are excellent scaffolds for various task-specific applications because of their high specific surface area, structural diversity and fine dispersion of catalytic sites [26, 27]. The lightweight, high intrinsic porosity and structural stability enhanced the great potential of these supports as heterogeneous organocatalysts. Thus, POPs are considered promising support materials [28, 29].

There are four categories of POPs, including hypercrosslinked polymers (HCPs), polymers of intrinsic microporosity (PIMs), covalent organic frameworks (COFs), and conjugated microporous polymers (CMPs) [30–34]. Among them, CMPs are organic porous materials that are composed of

completely conjugated molecular chains and have a microporous structure [35]. CMPs are used in many fields, including gas adsorption, heterogeneous catalysis, chemical sensing and energy conversion [22, 36–40]. CMPs exhibit several characteristics, including a large specific surface area, high stability, controllable and precise micropore size and volume, etc., showing great application potential in the field of catalysis [41]. Recently, the catalytic performance of many CMPs containing functional units, such as metalloporphyrins, bipyridines, triazines, and imines, has been enhanced by supporting Pd NPs on the framework [42–45]. The Pengyao Ju group prepared a salen-porphyrin-based CMP supporting Pd NPs heterogeneous catalyst (Pd@SP-CMP). For the Suzuki–Miyaura coupling reaction, Pd@SP-CMP showed good catalytic efficiency (78%–99% yield) and excellent stability in water or dioxane/water [46]. The Yaozu Liao group used nitrogen-rich CMPs to support Pd to prepare a heterogeneous catalyst with > 94% catalytic efficiency after 6 consecutive runs in the Suzuki–Miyaura coupling reaction [47]. The Lee group synthesized a CMP based on Pd acetylide from palladium dichloride and trialkyne. A heterogeneous catalyst supported by Pd NPs was synthesized via a one-step pyrolysis of Pd-CMP, producing a reaction yield higher than 95% for the Suzuki–Miyaura coupling reaction [48]. Pd supported on CMP has achieved good results in the catalysis of Suzuki–Miyaura coupling reaction. However, previous materials, such as porphyrin, are usually expensive, and the synthesis steps are complicated.

In this study, four kinds of CMPs with different numbers of aromatic nuclei and nitrogen atoms via imine bonds were designed and synthesized. The loading of Pd NPs on CMPs was discussed, and the catalytic efficiency of the four Pd/CMPs for Suzuki–Miyaura coupling reaction was confirmed. Finally, we proposed a rational catalytic cycle to provide a new idea for the structural design of CMP used as heterogeneous catalyst.

## Experimental

### Materials

3,5-Dibromobenzaldehyde (A2), triphenylphosphine, cuprous iodide, aniline, 8-aminoquinoline, *n*-

hexamine, palladium acetate and sodium borohydride were purchased from Shanghai Aladdin Biochemical Technology Co., Ltd. 1,3,5-Tris(4-ethynylphenyl)benzene (B3), 1,3,5-triethynylbenzene (B3s) and bis(triphenylphosphine)palladium dichloride were purchased from Shanghai McLean Biochemical Technology Co., Ltd. Unless otherwise stated, all the chemicals were used without purification and all polymers were synthesized under a nitrogen atmosphere.

## Characterizations

$^1\text{H}$ NMR spectra were obtained by using a 600 MHz Bruker AV600 + BH0055 superconducting NMR spectrometer. Using Bruker BL Tensor37 spectrometer, FT-IR spectral analysis was conducted in the range of 4000–400  $\text{cm}^{-1}$ . Using a 400 MHz Bruker AVANCE III HD NMR spectrometer,  $^{13}\text{C}$ NMR spectra were obtained. The American MAC ASAP 2460 system was used to measure nitrogen adsorption and desorption isotherms at 77 K, and the pore size distribution curve was calculated based on the nonlocal density functional theory (NLDFT). The ESCALAB250Xi Thermo spectrometer was used for XPS measurements. The NEXION350X PE ICP-MS spectrometer was used for confirming Pd contents. We obtained scanning electron microscopy (SEM) images by using a HITACHI S-4300 electron microscope. High-resolution transmission electron microscopy (HRTEM) and transmission electron microscopy (TEM) images were obtained with a Talos F200S. The EDS image was obtained with SUPERX. Using a France Setaram Labsys Evo thermogravimetric analyzer, thermogravimetric analysis (TGA) was performed. Using a D8, Bruker-AES, powder X-ray diffraction (PXRD) was performed. The reaction mixture was analyzed using a GC122 instrument (Shanghai Precision Scientific Instrument). GC conversion was determined by integrating the feedstock and product peaks using preestablished response factors.

## Synthesis of CMPs

### *Synthesis of CMPs with CHO groups (Scheme 1)*

3,5-Dibromobenzaldehyde (A2) (750 mg, 2.84 mmol), 1,3,5-tris(4-ethynylphenyl)benzene (B3) (717 mg, 1.89 mmol),  $\text{Pd}(\text{PPh}_3)_2\text{Cl}_2$  (99.6 mg, 0.14 mmol, 5%),

$\text{PPh}_3$  (372 mg, 1.42 mmol, 50%) and  $\text{CuI}$  (27.1 mg, 140  $\mu\text{mol}$ , 5%) were added to the reaction flask, triethylamine (90.0 mL) was injected under a nitrogen atmosphere, and under reflux the reaction was carried out for 24 h. When the system is cooled to room temperature, the crude product was washed successively with three solvents (toluene, chloroform and KI aqueous solution), then extracted with dichloromethane Soxhlet for 24 h and vacuum-dried for 36 h. The yellow powder obtained was CMP1 with a yield of 98.8%.

The synthesis process of CMP2 is similar to that of CMP1. The light yellow powder obtained was CMP2 with a yield of 99.1%.

### *Synthesis of CMPs with imine groups (Scheme 1)*

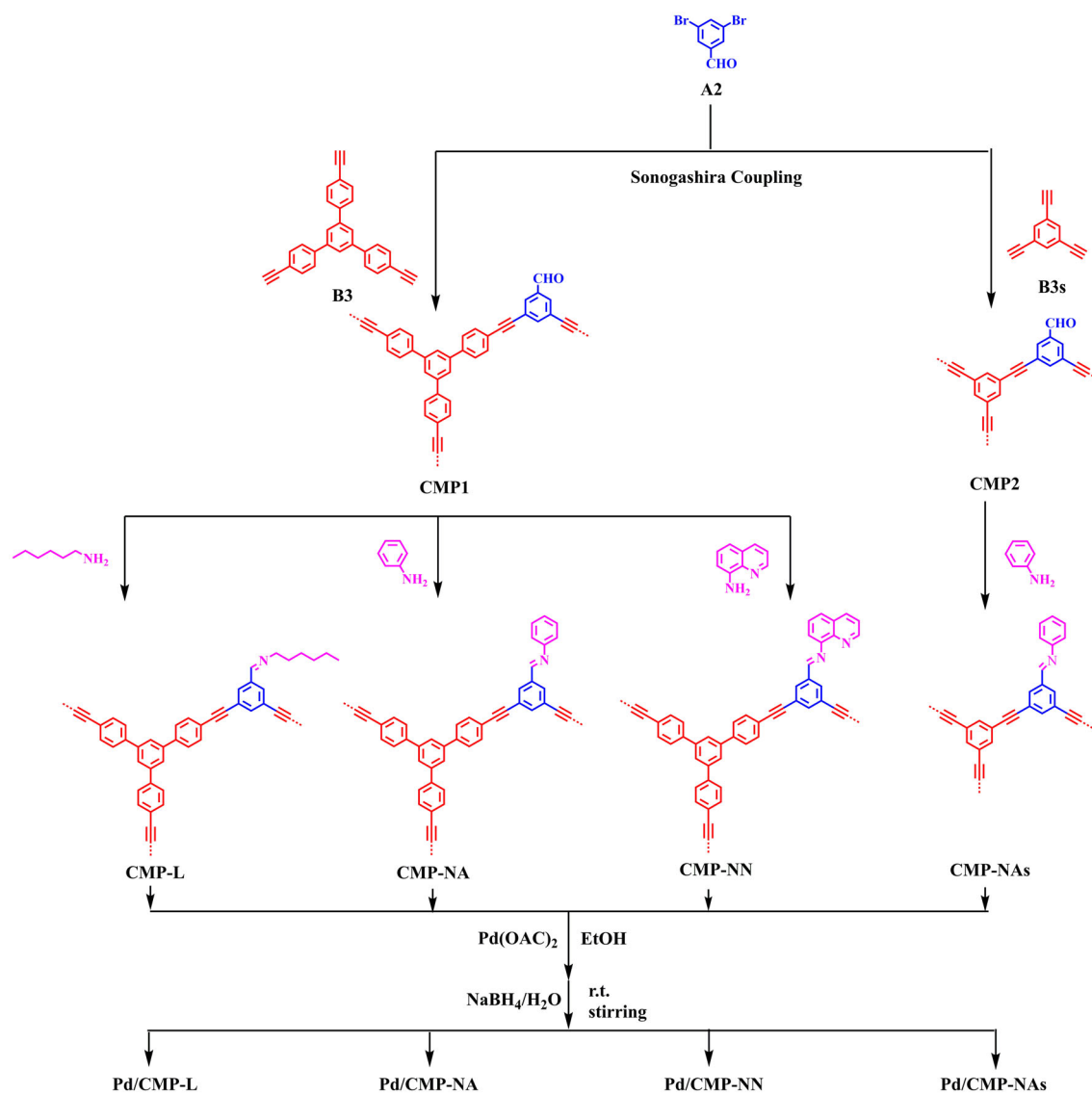
CMP1 (164 mg, 300  $\mu\text{mol}$ ) and aniline (27.9 mg, 300  $\mu\text{mol}$ ) were added to the reaction flask, and N,N-dimethylformamide (10.0 mL) was injected. The reaction was carried out at 120  $^\circ\text{C}$  for 48 h. When the system was cooled to room temperature, the reaction was removed and filtered. The crude product was washed with solvent until the filtrate was colorless. After extraction with dichloromethane Soxhlet for 24 h and drying in vacuum for 24 h, the orange powder obtained was CMP-NA with a yield of 83.0%.

The process of synthesizing CMP-L, CMP-NN and CMP-NAs was similar to that of CMP-NA, and yields of 89.5%, 85.7% and 80.2% were obtained, respectively.

### *Synthesis of Pd/CMPs (Scheme 1)*

CMP-NA (30.0 mg) was added to palladium acetate (9.00 mg, 400  $\mu\text{mol}$ ) in ethanol (3.00 mL), and stirred for 12 h at room temperature. The solid obtained was separated by centrifugation and washed with acetonitrile. The obtained solid was added to a 4 mL solution of sodium borohydride (46.8 mg, 1.24 mmol) (water/ethanol (v:v) = 1:1) and stirred for another 8 h at room temperature. After filtering the solid, it was washed with deionized water and ethanol and dried for 24 h in vacuum. The dark brown powder obtained was Pd/CMP-NA with a yield of 91.5%.

The process of synthesizing Pd/CMP-L, Pd/CMP-NN and Pd/CMP-NAs was the same as that of Pd/CMP-NA. The three kinds of Pd/CMPs were dark brown powders, and the yields were 90.2%, 94.1% and 90.2%, respectively.



**Scheme 1** Synthesis route of CMPs and Pd/CMPs.

### Experimental process of Suzuki–Miyaura coupling reaction

Typically, phenylboronic acid (750  $\mu\text{mol}$ ), halobenzenes (500  $\mu\text{mol}$ ), Pd/CMP-NA (0.75 mol%) and NaOH (750  $\mu\text{mol}$ ) were added to the reaction flask, and the mixture was stirred in solvent (3.00 mL) for 1 h under 80 °C and nitrogen atmosphere. After cooling the system to room temperature, the catalyst was filtered and washed with ethyl acetate several times, then dried and put into for the next cycle. The organic layer was extracted and collected, the solvent was evaporated in vacuum after water removal, and the crude product was purified by column chromatography.

### Results and discussion

#### Synthesis process of CMPs containing imine groups with different numbers of aromatic nuclei and nitrogen atoms

CMP1 and CMP2 were synthesized by a Sonogashira coupling reaction according to Scheme 1 as a material for synthesizing CMPs with imine groups. The structures of CMP1 and CMP2 were confirmed by FT-IR spectra. The stretching vibration peak of  $-\text{C}\equiv\text{C}-\text{H}$  at  $3274\text{ cm}^{-1}$  disappeared, which was attributed to monomers B3 and B3s; a new peak of  $-\text{C}\equiv\text{C}-$  was generated at  $2203\text{ cm}^{-1}$ ; and the stretching vibration peak of  $-\text{C}=\text{O}$  at  $1697\text{ cm}^{-1}$  remained,

which was attributed to monomer A2 (Fig. S1(a, b)), indicating that the two CMPs with CHO groups were successfully synthesized.

Four kinds of CMPs with different numbers of aromatic nuclei and nitrogen atoms via imine groups (CMP-L, CMP-NA, CMP-NN, CMP-NAs) were prepared by postreaction of CMPs containing CHO groups with three kinds of amines (Scheme 1). The structures of CMPs with imine groups were determined by FT-IR and solid-state  $^{13}\text{C}$ -NMR. Stretching vibration peaks of  $-\text{C}\equiv\text{C}-$  at  $2203\text{ cm}^{-1}$  and a new peak of  $-\text{C}=\text{N}$  at  $1639\text{ cm}^{-1}$  were observed. The double peaks of  $-\text{NH}_2$  at  $3367$  and  $3282\text{ cm}^{-1}$  disappeared, and the stretching vibration peaks of  $-\text{C}=\text{O}$  at  $1697\text{ cm}^{-1}$  remained (Fig. 1a). Combined with the solid-state  $^{13}\text{C}$ -NMR spectrum, in which the peaks of  $-\text{C}\equiv\text{C}-$  and  $-\text{C}=\text{N}$  at  $90.4$  and  $158.3\text{ ppm}$  were

observed (Fig. 2), the results indicated that CMP-L was successfully synthesized. Similarly, from the FT-IR spectra of the other three CMPs with imine structures (CMP-NA, CMP-NN, CMP-NAs), the stretching vibration peaks of  $-\text{C}=\text{N}$  were generated (Fig. 1b, c, d), and their solid-state  $^{13}\text{C}$ -NMR spectra showed the peaks of  $-\text{C}\equiv\text{C}-$  and  $-\text{C}=\text{N}$  (Fig. 2). We can conclude that all CMPs with different numbers of aromatic nuclei and nitrogen atoms via imine groups were synthesized successfully.

X-ray photoelectron spectroscopy (XPS) was used to measure the elemental composition in the CMPs with imine groups. Taking CMP-NA as an example, the C 1s and N 1s peaks at  $283.1$  and  $397.1\text{ eV}$  were observed in the survey spectra (Fig. S2 (a)). The different binding energies in the C 1s spectrum at  $284.4$ ,  $284.7$ ,  $284.9$  and  $285.5\text{ eV}$  were attributed to C-H,

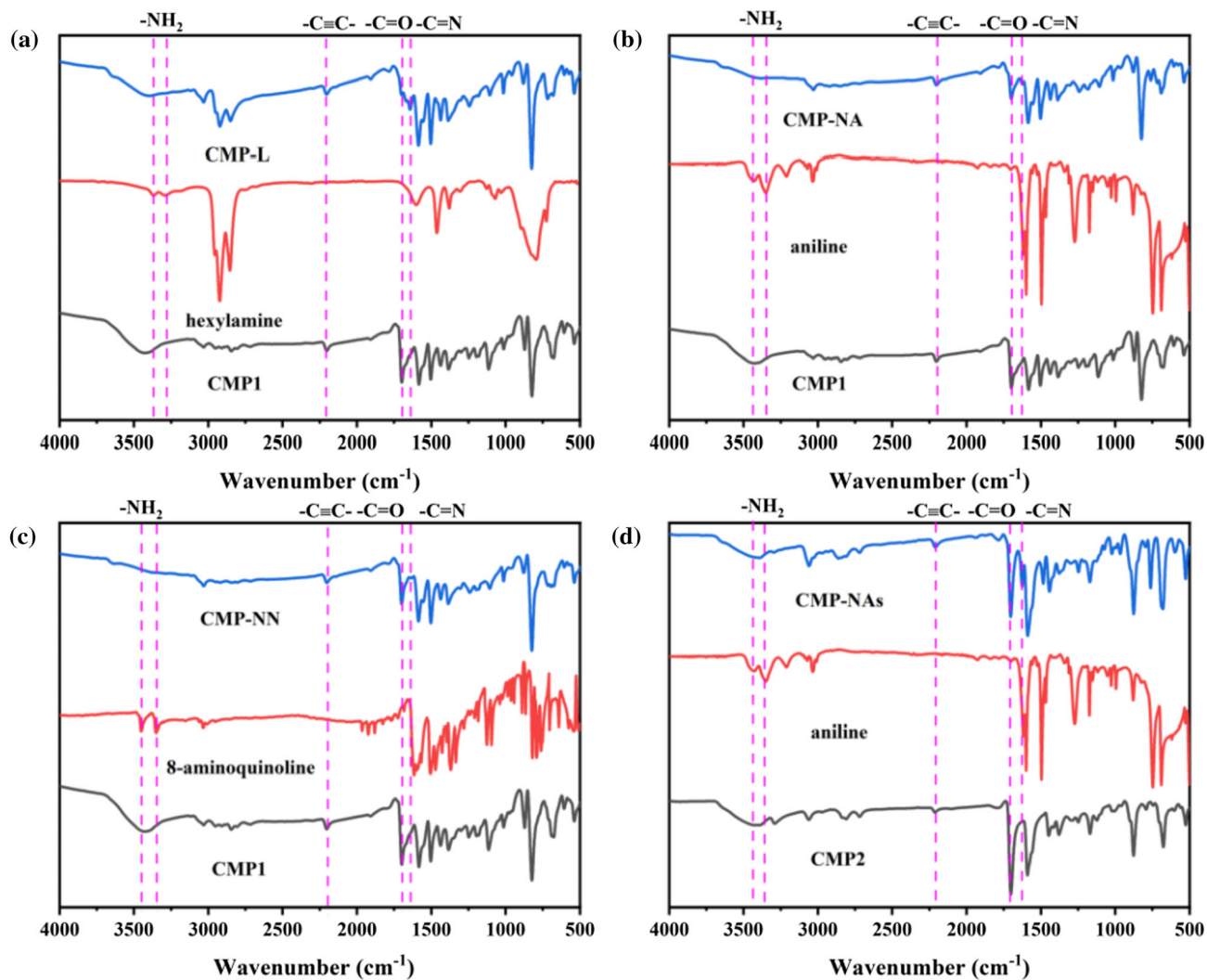


**Figure 1** FT-IR spectra of **a** CMP-L, **b** CMP-NA, **c** CMP-NN, and **d** CMP-NAs.



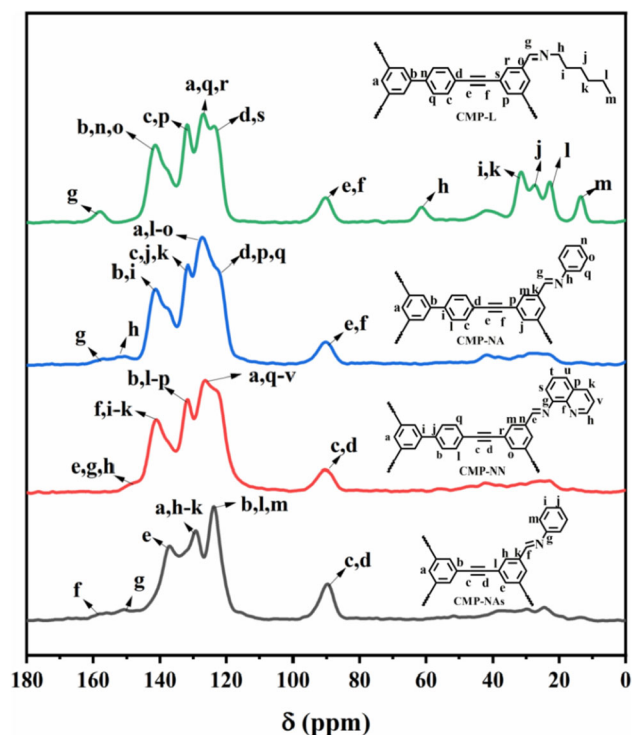


**Figure 2** Solid-state  $^{13}\text{C}$ -NMR spectrum of CMPs with imine structures.

C = N, C–C and C–N, respectively (Fig. 3a). In the N 1s spectrum (Fig. 3(b)), two different binding energies at 399.6 and 400.5 eV were arisen from the C–N and C = N bonds. All results further confirmed that CMP-NA was synthesized successfully. The XPS spectra of other CMPs having imine groups were shown in Figs. S2–S5.

The porosity of CMPs with imine structures was obtained by  $\text{N}_2$  adsorption/desorption isotherms

(Fig. 4 and insets), and we calculated the pore size distribution by the nonlocal density functional theory (NL-DFT) method. The adsorption curves of two kinds of CMPs exhibited a type I sorption profile. The Brunauer–Emmett–Teller (BET) surface areas of CMP-NA and CMP-NAs were 74.8 and 73.5  $\text{m}^2/\text{g}$ , and the pore size distribution was narrow at 1.4 and 1.5 nm, respectively. The low BET surface areas of CMP with imine groups may be because of the large steric hindrance between the postsynthesized imine part and the CMPs that contained a CHO group skeleton. The morphology of CMPs with imine structures was characterized by SEM (Fig. 5a). The CMPs with a large skeleton of B3 showed regular sphere morphologies, while CMP-NAs with a small skeleton of B3s did not show regular morphology. Thermogravimetric (TG) analysis was carried out to test the thermal stability of CMP-NA (Fig. S6). CMP-NA started to decompose at 200  $^\circ\text{C}$  and showed a weight loss of 3.1% at approximately 300  $^\circ\text{C}$ , which may be due to the small molecules left in the pores of CMPs. CMP-NA remained 71.3% at 800  $^\circ\text{C}$ , which suggested its good thermal stability.

### Synthesis of the Pd/CMP heterogeneous catalyst

Four kinds of Pd/CMP heterogeneous catalysts (Pd/CMP-L, Pd/CMP-NA, Pd/CMP-NN, Pd/CMP-NAs) with different Pd contents were synthesized by treating CMPs with palladium acetate followed by reduction with sodium borohydride (Scheme 1). The morphology of Pd/CMPs showed almost no change

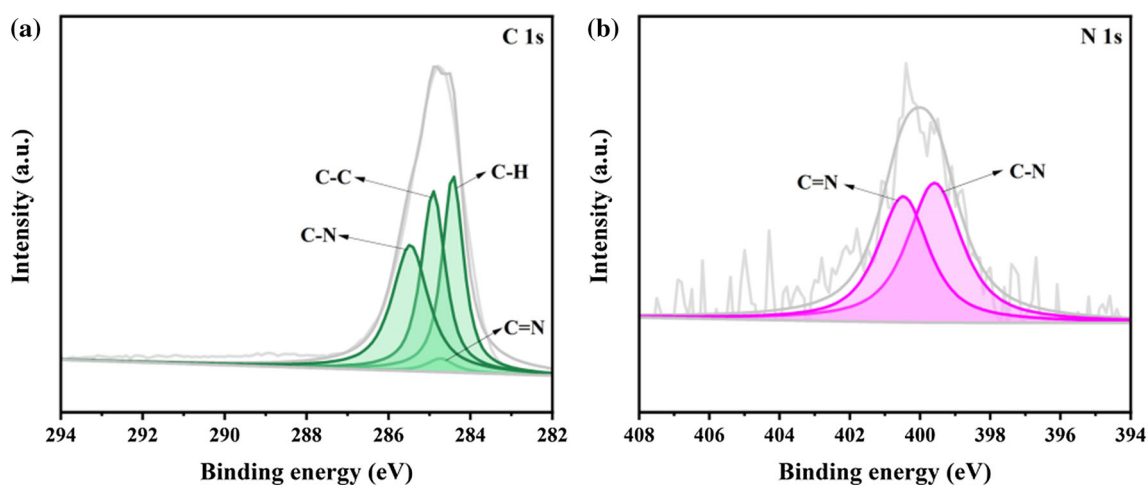


**Figure 3** a C 1s XPS spectrum of CMP-NA, b N 1s XPS spectrum of CMP-NA.

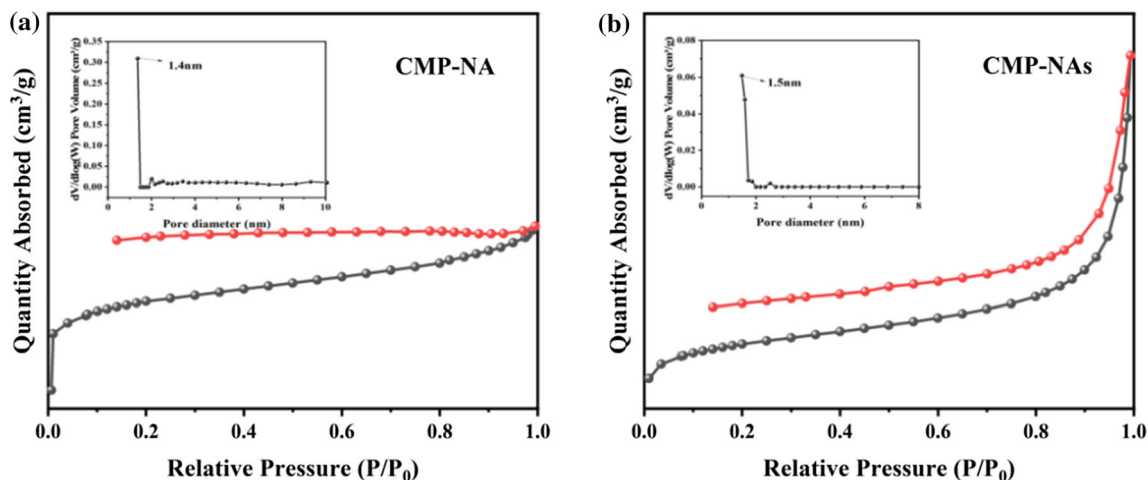


**Figure 4** The  $N_2$  adsorption–desorption and pore-size distribution curves of **a** CMP-NA, **b** CMP-NAs.

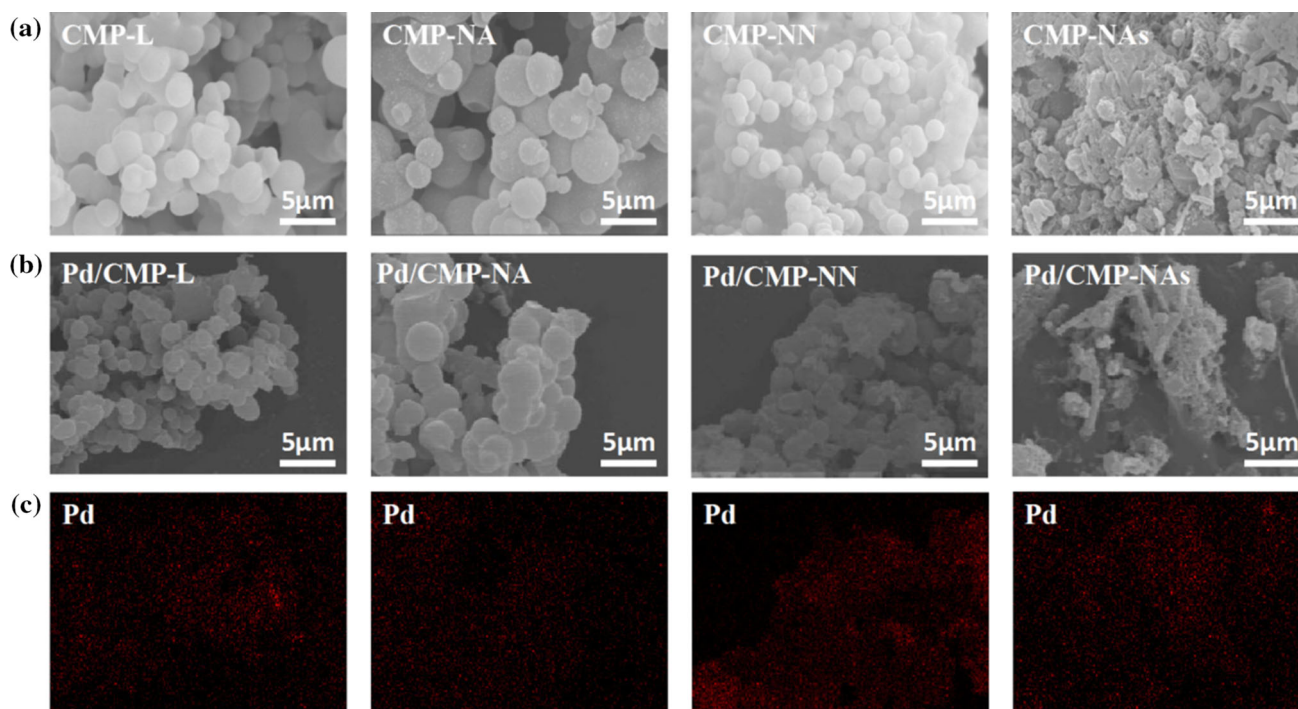


**Figure 5** **a** SEM images of CMP-L, CMP-NA, CMP-NN and CMP-NAs from left to right, **b** SEM images and **c** EDS SEM mapping for Pd element images of Pd/CMP-L, Pd/CMP-NA, Pd/CMP-NN and Pd/CMP-NAs from left to right.

compared with that of CMPs (Fig. 5b). Judging from the EDS SEM-mapping images (Fig. 5c) and the TEM image (Fig. 6a), the Pd NPs were more uniformly dispersed in CMP-NA and CMP-NAs, and there was a small amount of Pd aggregation in Pd/CMP-L and Pd/CMP-NN. To further confirm the crystalline diffraction of Pd NPs, HR-TEM was performed. The Pd NPs were in the crystalline phase with an interplanar spacing of 0.231 nm, corresponding to the

(111) plane of Pd NPs (Fig. 6b). The characteristic diffraction plane at (111) was given in the corresponding selected area electron diffraction (SAED) pattern (Fig. 6c). The high-annular dark-field scanning TEM (HAADF-STEM) pattern (Figs. 6d and e) and the elemental mapping of Pd (Fig. 6f) further demonstrated that the Pd NPs were uniformly dispersed.

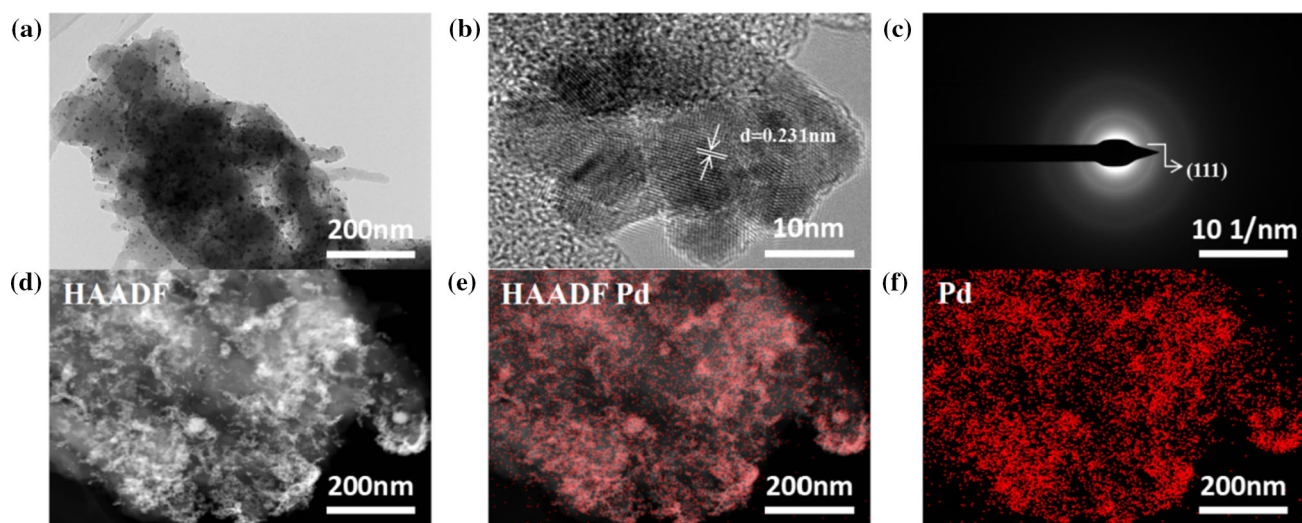


**Figure 6** **a** TEM images of CMP-NAs, **b** HR-TEM images of CMP-NAs, **c** selected-area electron diffraction (SAED) images of CMP-NAs, **d** high-annular dark-field scanning TEM (HAADF-

STEM) images of CMP-NAs, **e** HAADF Pd images of CMP-NAs, and **f** EDS TEM mapping for Pd element images of CMP-NAs.

XPS was used to reveal the interaction between Pd and CMPs, and the oxidation state of Pd in Pd/CMPs can be confirmed. In the XPS survey spectrum, the diffraction peak of Pd was found at a binding energy of 336.3 eV (Figs. S2(a)–(d)), and the N1s XPS spectra showed the N–Pd peak at a binding energy of 399.1 eV (Figs. 7a and S7–S9(a)). The results above indicated that the Pd NPs were successfully immobilized on CMPs through imine groups. The Pd 3d XPS spectra (Figs. 7b and S7–S9(b)) showed that the binding energies of 335.0 and 340.3 eV were the diffraction peaks of Pd 3d<sup>5/2</sup> and Pd 3d<sup>3/2</sup>, proving that the Pd in Pd/CMPs was Pd(0). The XRD patterns of Pd/CMPs showed a wide diffraction peak at 20.68° from the CMPs and sharp peaks at 39.26°, 45.62°, 66.62° and 80.34°, corresponding to the (111), (200), (220) and (311) crystal planes of Pd, respectively (Figs. 7c and S7–S9(c)). The FT-IR spectra of CMPs and Pd/CMPs were measured (Figs. 7d and S7–S9(d)). The stretching vibration peak of –C = N shifted from 1626–1639 to 1551–1552 cm<sup>-1</sup> after immobilizing Pd on CMPs, which further proved the successful synthesis of Pd/CMPs [49]. The Pd contents of Pd/CMPs were confirmed by using ICP-MS (Table 1). The CMP-NN with two aromatic nuclei and two nitrogen atoms supported the most Pd, which may be caused by the stronger  $\pi$ – $\pi$  stacking interaction and the greater number of sites for Pd to be immobilized.

### Catalytic efficiency of Pd/CMPs in the Suzuki–Miyaura model reaction

#### Optimization of the model reaction using Pd/CMP-NA

To evaluate the catalytic efficiency of Pd/CMPs as heterogeneous catalysts for the Suzuki–Miyaura coupling reaction, the phenylboronic acid and *p*-iodotoluene as model reactions using Pd/CMP-NA was utilized (Scheme 2). We systematically studied the effects of reaction time, base, base content, solvent and temperature on the catalytic efficiency of Pd/CMP-NA, and the results were shown in Fig. 8 and Table 2. The conversion increased rapidly during the first 5 min, and when the reaction time was extended to 1 h, the conversion reached 99.0% (Fig. 8). In addition, considering that bases exert a significant effect, organic bases (Et<sub>3</sub>N, tBuOK) and inorganic bases (Na<sub>2</sub>CO<sub>3</sub>, K<sub>3</sub>PO<sub>4</sub>·3H<sub>2</sub>O, NaOH) were also tested. In the model reaction, NaOH showed the best yield of 82.6% with a TON of 82.6. when the concentration was 1.5 eq (Table 2, entries 1–8), and inorganic bases with stronger basicity led to higher reactivity. Both aprotic and protic solvents were used as solvents in the model reaction (Table 2, entries 5, 9–12), and the two-component solvent EtOH/H<sub>2</sub>O showed the best performance, yielding 90.2% of the target product (Table 2, entry 12). This may be attributed to the presence of hydroxyl groups in the alcohol molecule, as these groups provide a hydrogen bond donor, which facilitates the C–I bond



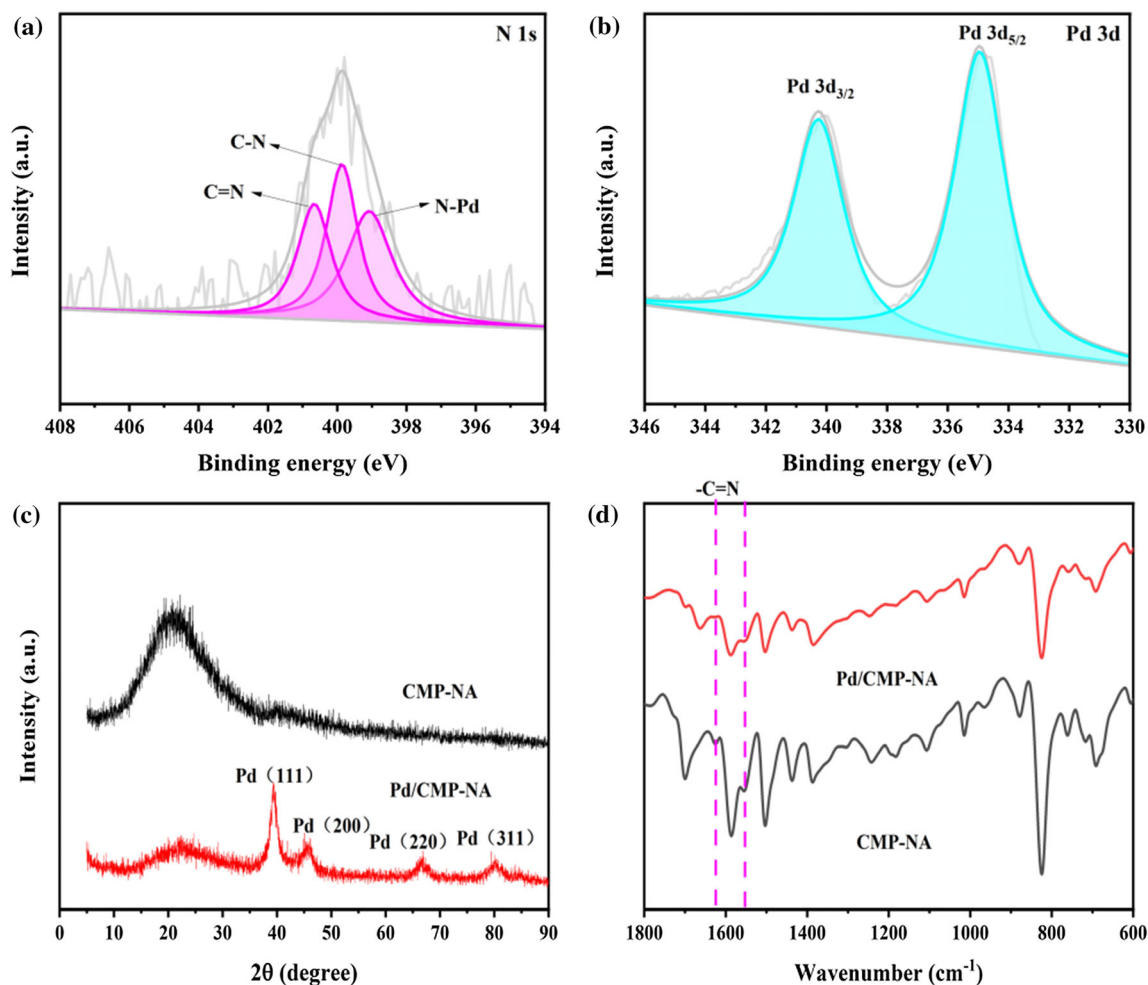


**Figure 7** a N 1s XPS spectrum of Pd/CMP-NA, b Pd 3d XPS spectrum of Pd/CMP-NA, c XRD patterns of CMP-NA and Pd/CMP-NA, d FT-IR spectra of CMP-NA and Pd/CMP-NA.

**Table 1** Pd contents of the Pd/CMPs by ICP-MS

Pd/CMP	Pd infeed <sup>a</sup> (wt %)	Pd content <sup>b</sup> (wt %)
Pd/CMP-NA	10	3.06
Pd/CMP-NA	20	5.68
Pd/CMP-NA	30	7.92
Pd/CMP-L	30	6.70
Pd/CMP-NN	30	8.54
Pd/CMP-NAs	30	7.76

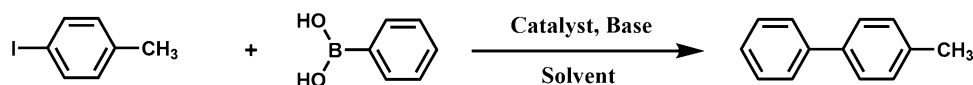
<sup>a</sup> $W_{\text{Pd(OAC)}_2}/W_{\text{CMPs}} \times 100\%$

<sup>b</sup>Pd content in Pd/CMPs measured by ICP-MS

dissociation of the halide and facilitated the coupling reaction [49]. In conclusion, the best reaction conditions for Suzuki–Miyaura coupling using Pd/CMP-NA as a heterogeneous catalyst were confirmed: 1.5 eq NaOH was used as the base, and the reaction was carried out in EtOH/H<sub>2</sub>O at 80 °C for 1 h (Table 2, entry 9).

#### Effect of Pd content on Suzuki–Miyaura model reaction

The yield of the Suzuki–Miyaura coupling reaction was greatly affected by the Pd content. When CMP-



**Scheme 2** Suzuki–Miyaura model reaction of *p*-iodotoluene with phenylboronic acid.

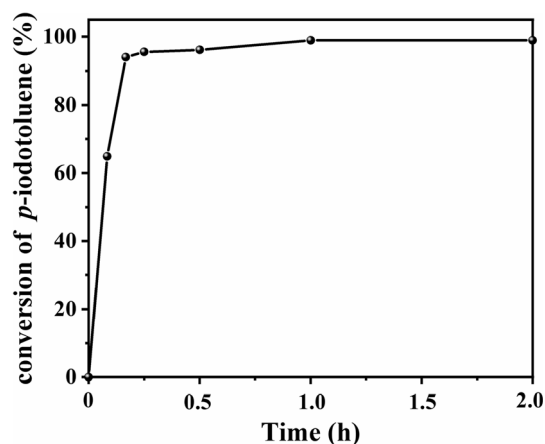


**Figure 8** The conversion curve of *p*-iodotoluene in Suzuki–Miyaura model reaction using Pd/CMP-NA as a heterogeneous catalyst.

NA loaded with different contents of Pd (0.29 mol% ~ 0.75 mol%) was used as the catalyst, the higher Pd contents produced a higher yield (Table 3, entries 1–3). However, as the Pd content increased from 0.75 mol% to 1.0 mol%, the yield showed almost no change (Table 3, entry 4). Therefore, a Pd/CMP-NA with Pd content of 0.75 mol% is sufficient for catalyzing the Suzuki–Miyaura model reaction. In order to confirm the role of Pd NPs

loaded on the CMPs, CMP-NA without Pd NPs was used as catalyst for Suzuki–Miyaura model reaction, and almost no corresponding catalytic product can be obtained (Table S1, entry 1).

#### *Effect of the chemical structure of CMPs on the Suzuki–Miyaura model reaction*

The effect of Pd/CMPs with different substituents with the same Pd content on the model reaction was discussed (Table 3, entries 4–6, Table S1). Pd/CMP-NA showed the highest catalytic efficiency with a yield of 94.3%. This may be because compared to the other Pd/CMPs, the Pd NPs in Pd/CMP-NA were dispersed more uniformly (Fig. 5(c)) and exhibited higher atom utilization, which led to higher catalytic efficiency [50]. We also discussed the effect of skeleton size on catalysis (Table 3, entries 4 and 7), the Pd/CMP-NA with large skeleton showed higher catalytic efficiency. This may be caused by the higher specific surface area of Pd/CMP-NA with large skeleton, which increased the reactive surface of the catalyst.

**Table 2** Suzuki–Miyaura model reactions of phenylboronic acid and *p*-iodotoluene using Pd/CMP-NA as catalyst<sup>a</sup>

Entry	Solvent <sup>b</sup>	Base	Dosage (equiv.)	Temperature (°C)	Time (h)	Yield <sup>c</sup> (%)	TON <sup>d</sup>
1	DMF/H <sub>2</sub> O	Et <sub>3</sub> N	1.5	80	1	28.4	28.4
2	DMF/H <sub>2</sub> O	tBuOK	1.5	80	1	71.8	71.8
3	DMF/H <sub>2</sub> O	Na <sub>2</sub> CO <sub>3</sub>	1.5	80	1	47.7	47.7
4	DMF/H <sub>2</sub> O	K <sub>3</sub> PO <sub>4</sub> ·3H <sub>2</sub> O	1.5	80	1	76.7	76.7
5	DMF/H <sub>2</sub> O	NaOH	1.5	80	1	82.6	82.6
6	DMF/H <sub>2</sub> O	NaOH	1.0	80	1	55.9	55.9
7	DMF/H <sub>2</sub> O	NaOH	2.0	80	1	69.3	69.3
8	DMF/H <sub>2</sub> O	NaOH	2.5	80	1	68.9	68.9
9	EtOH/H <sub>2</sub> O	NaOH	1.5	80	1	90.2	90.2
10	1,4-Dioxane/H <sub>2</sub> O	NaOH	1.5	80	1	69.3	69.3
11	DMF	NaOH	1.5	80	1	29.2	29.2
12	Toluene	NaOH	1.5	80	1	31.1	31.1
13	EtOH/H <sub>2</sub> O	NaOH	1.5	RT	4	77.4	77.4
14	EtOH/H <sub>2</sub> O	NaOH	1.5	50	1.5	77.2	77.2
15	EtOH/H <sub>2</sub> O	NaOH	1.5	120	0.17	62.2	62.2

<sup>a</sup>*p*-iodotoluene (500 μmol), phenylboronic acid (750 μmol), solvent (3.00 mL), Pd/CMP-NA (1.0 mol% Pd content), N<sub>2</sub>

<sup>b</sup>The volume ratio of two components solvent was 1:1

<sup>c</sup>Isolated yields based on *p*-iodotoluene

<sup>d</sup>TON = (moles of product)/(moles of metal in the catalyst)

**Table 3** Suzuki–Miyaura model reactions of phenylboronic acid and *p*-iodotoluene catalyzed by Pd/CMPs<sup>a</sup>

Entry	Catalyst	Pd content <sup>b</sup> (mol%)	Yield <sup>c</sup> (%)	TON <sup>d</sup>
1	Pd/CMP-NA	0.29	41.5	143
2	Pd/CMP-NA	0.54	65.2	121
3	Pd/CMP-NA	0.75	94.9	127
4	Pd/CMP-NA	1.0	94.3	94.3
5	Pd/CMP-L	1.0	82.4	82.4
6	Pd/CMP-NN	1.0	76.8	76.8
7	Pd/CMP-NAs	1.0	90.2	90.2

<sup>a</sup>*p*-iodotoluene (500 μmol), phenylboronic acid (750 μmol), NaOH (750 μmol), 80 °C, N<sub>2</sub>, 1 h

<sup>b</sup>Pd content (Pd mole/substrate mole)

<sup>c</sup>Isolated yields based on *p*-iodotoluene

<sup>d</sup>TON = (moles of product)/(moles of metal in the catalyst)

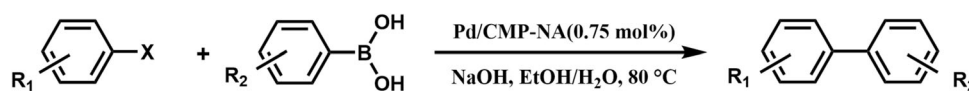
### Suzuki–Miyaura coupling reaction of various substrates catalyzed by Pd/CMP-NA

We tested various substituted aryl halides and phenylboronic acids to explore the versatility of the catalytic system. The Suzuki–Miyaura reaction between various substrates using Pd/CMP-NA

under the optimal reaction conditions (Scheme 3) was carried out. The catalytic conversion was up to 100%, and the yield reached 95.4% with a TON of 127. The reactivity of substituted iodobenzene was higher than that of substituted bromobenzene (Table 4, entries 1–4) and obtained higher conversions (greater than 99.0%). In addition, the introduction of electron-donating groups to iodobenzene decreased the conversion of Suzuki–Miyaura coupling reaction (Table 4, entries 4–6). On the other hand, when an electron withdrawing group (either ortho- or para-substituted) was introduced to iodobenzene, 100% conversion was achieved (Table 4, entries 7 and 8). Furthermore, the conversion was slightly reduced (83.5% and 91.5%) for the substituted phenylboronic acids containing electron-donating or electron-withdrawing groups (Table 4, entries 9, 10).

### The heterogeneity test of Pd/CMP-NA

The heterogeneity of Pd/CMP-NA was demonstrated by hot filtration experiments (Fig. S10). The Pd/CMP-NA was filtered out when the reaction was performed at 80 °C for 20 min, and the filtrate was taken to measure the 98.6% conversion by GC. The

**Scheme 3** Suzuki–Miyaura coupling reaction synthesis of different halogenated benzene with different phenylboronic acids.**Table 4** Suzuki–Miyaura coupling reactions of different substrates using Pd/CMP-NA heterogeneous catalyst<sup>a</sup>

Entry	R1	X	R2	Time (h)	Conversion <sup>b</sup> (%)	Yield <sup>c</sup> (%)	TON <sup>d</sup>
1	H	Br	H	2	95.1	81.2	108
2	<i>p</i> -Me	Br	H	2	86.5	80.0	107
3	H	I	H	1	100	95.1	127
4	<i>p</i> -Me	I	H	1	99.0	94.9	127
5	<i>p</i> -OMe	I	H	1	91.6	85.8	114
6	<i>p</i> -NH <sub>2</sub>	I	H	1	92.5	83.9	112
7	<i>p</i> -NO <sub>2</sub>	I	H	1	100	95.4	127
8	<i>o</i> -NO <sub>2</sub>	I	H	1	100	92.3	123
9	<i>p</i> -Me	I	<i>m</i> -OMe	1	91.5	81.7	109
10	<i>p</i> -Me	I	<i>p</i> -CHO	1	83.5	72.1	96

<sup>a</sup>Aryl halides (500 μmol), Arylboronic acids (750 μmol), NaOH (750 μmol), EtOH:H<sub>2</sub>O = 1:1 (V:V), 3.00 mL, and Pd/CMP-NA (0.75 mol% Pd content)

<sup>b</sup>The conversion is determined by GC

<sup>c</sup>Isolated yield based on aryl halides

<sup>d</sup>TON = (moles of product)/(moles of metal in the catalyst)

filtrate was further heated under the same reaction conditions for 2 h without obtaining any coupling product. The Pd/CMP-NA was added again to continue the reaction for 2 h, and the conversion was increased to 100%, as measured by GC. These results clearly indicated that Pd/CMP-NA was a heterogeneous catalyst and that a catalytic reaction carried out by dissolved homogeneous Pd did not occur.

#### Cyclic characteristics of the Pd/CMP-NA heterogeneous catalysts

The stability and recyclability of Pd/CMP-NA as a heterogeneous catalyst for the Suzuki–Miyaura coupling reaction were discussed. The conversion showed almost no change after two cycles and was maintained at more than 80% after 5 cycles (Fig. 9a). The slight drop in conversion was due to the slight exfoliation of Pd caused by vigorous stirring during the catalytic process (Fig. 9b). The structure and metal valence states of the reused Pd/CMP-NA were also investigated. The FT-IR spectrum (Fig. S11) of Pd/CMP-NA did not change after 5 catalytic cycles, and the Pd 3d XPS spectrum (Fig. S12) showed binding energies of Pd 3d<sup>5/2</sup> and Pd 3d<sup>3/2</sup> at 335.0 and 340.3 eV, respectively, indicating that the Pd in Pd/CMP-NA remained Pd(0). TEM images showed that after 5 cycles, Pd NPs in Pd/CMP-NA were uniformly dispersed without obvious aggregation (Fig. S13). SEM images showed that the morphology of Pd/CMP-NA did not change after 5 cycles (Fig. S14). The stability of Pd/CMP-NA as a

heterogeneous catalyst for the Suzuki–Miyaura coupling reaction was very high.

#### Suzuki–Miyaura coupling reaction mechanism using Pd/CMPs as catalysts

The possible mechanism the Suzuki–Miyaura coupling reaction by using Pd/CMP-NA catalyst was shown in Scheme 4. The Pd(0) supported on CMP-NA underwent an oxidative addition reaction with halogenated aromatic hydrocarbons to form the complex (A) of Pd(II) and then underwent a metal transfer reaction with alkali-activated phenylboronic acid to form the complex (B) of Pd(II), and finally, reductive elimination afforded the product and Pd/CMP-NA, which was consistent with the mechanism reported in a previous article [51].

## Conclusions

In summary, four kinds of Pd/CMPs with different Pd contents were synthesized and used as heterogeneous catalysts for the Suzuki–Miyaura coupling reaction. More Pd can be loaded with stronger  $\pi$ – $\pi$  stacking interaction and greater numbers of nitrogen atoms in the CMP support. The Pd/CMP-NA with good Pd NPs dispersibility and appropriate Pd content showed the best catalytic efficiency with a yield of 95.4% and a conversion of 100% in the Suzuki–Miyaura coupling reaction. The Pd/CMPs showed good substrate adaptability and recyclability, and the yield was maintained at 80.2% after 5 cycles. To

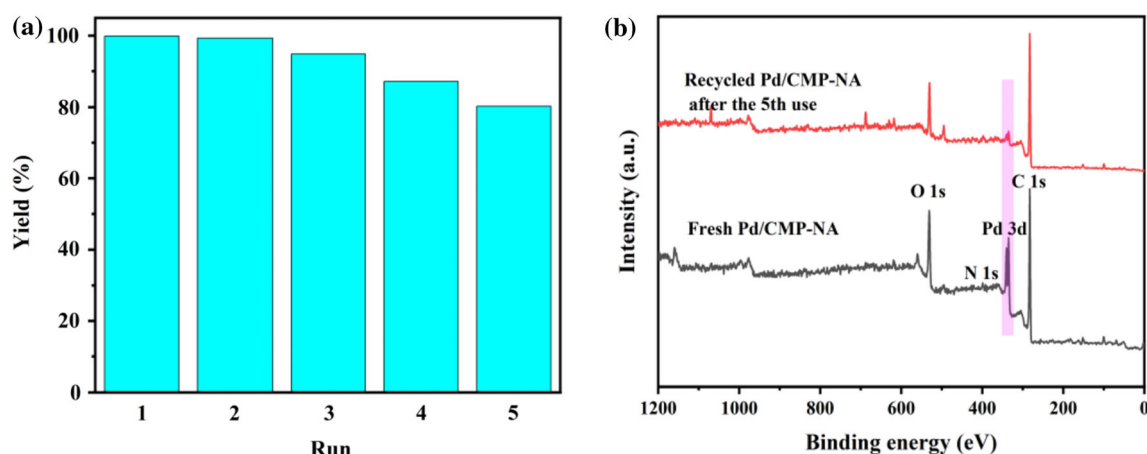
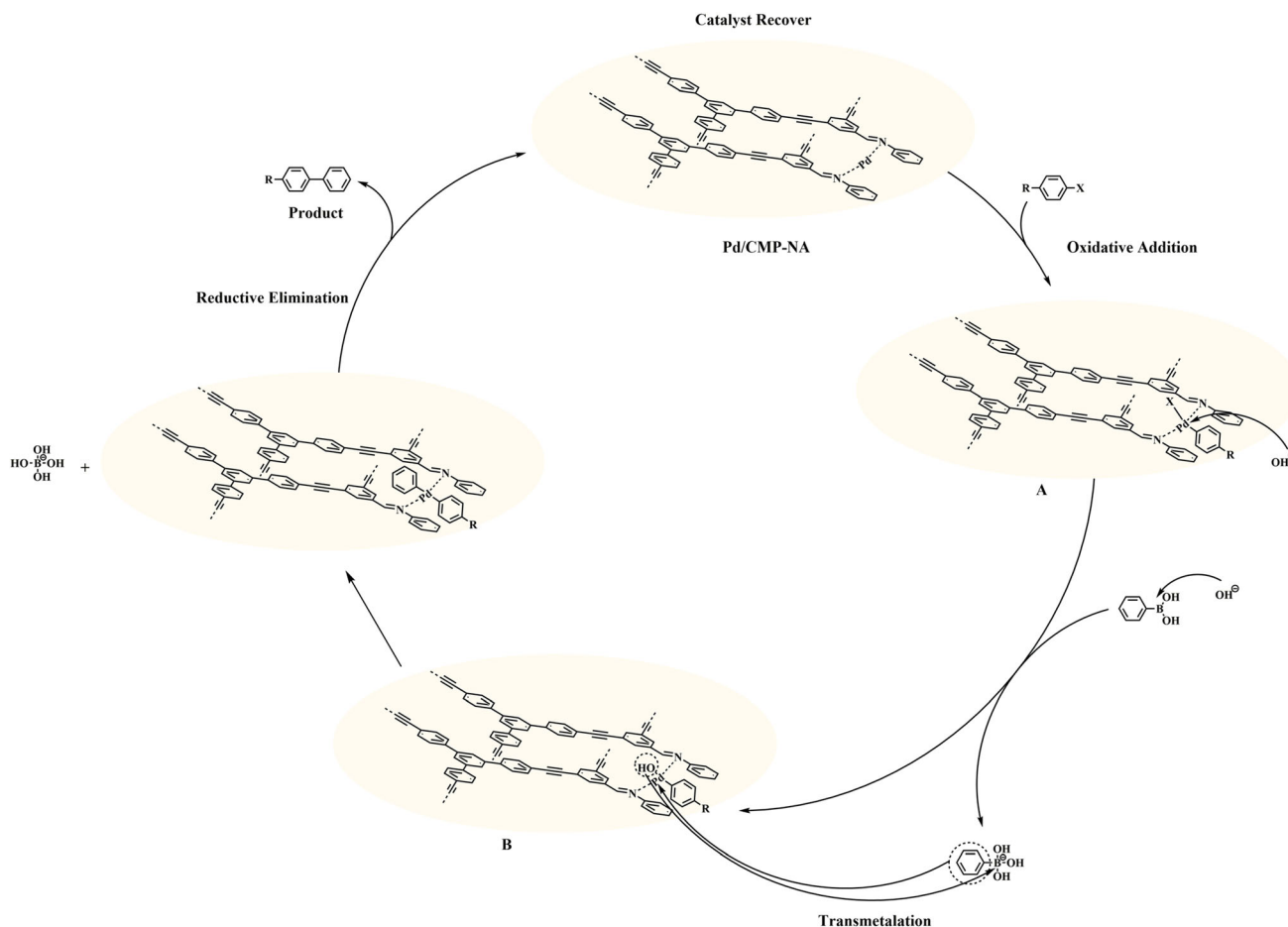


**Figure 9** **a** Recycling catalytic test for the Suzuki–Miyaura model reaction, **b** XPS survey spectrum of Pd/CMP-NA (black line) and Pd/CMP-NA after the five runs of catalysis (red line).





**Scheme 4** Probable mechanism of Pd/CMP-NA catalyzed Suzuki–Miyaura coupling reaction.

further understand the catalytic mechanism of Pd/CMP-NA in the Suzuki–Miyaura coupling reaction, we proposed a rational catalytic cycle. This study revealed the structural design of the CMP-catalyzed Suzuki–Miyaura coupling reaction.

### Acknowledgements

This research was funded by the National Natural Science Foundation of China, grant number 52173202; the Heilongjiang Science Foundation Project, grants number YQ2022116; the Fundamental Research Funds in Heilongjiang Provincial universities (135309348).

### Author's contribution

Y.Z. performed writing—review and editing. S.G. performed writing—original draft. B.J., H.S., J.W.,

J.L., and F.M. performed data curation. L.X. contributed to methodology and data curation.

### Data and code availability

Not applicable.

### Declarations

**Conflict of interest** The authors declare that they have no known competing financial interests or personal relationships that could have appeared to influence the work reported in this paper.

**Ethical approval** Not applicable.

**Supplementary Information:** The online version contains supplementary material available at <http://doi.org/10.1007/s10853-022-08032-8>.

## References

- [1] Kozuch S, Martin J (2011) What makes for a bad catalytic cycle? a theoretical study on the SuzukiMiyaura reaction within the energetic span model. *ACS Catal* 1:246–253. <https://doi.org/10.1021/cs100129u>
- [2] Miyaura N, Yamada K, Suzuki A (1979) A new stereospecific cross-coupling by the palladium-catalyzed reaction of 1-alkenylboranes with 1-alkenyl or 1-alkynyl halides. *Org Lett* 20:3437–3440. <https://doi.org/10.1021/ol10102085>
- [3] Jacquemin M, Hauwaert D, Debecker DP, Gaigneaux EM (2016) Influence of the acidity of oxidized Pd/silica-alumina catalysts on their performances in the Suzuki coupling. *J Mol Catal A-Chem* 416:47–55. <https://doi.org/10.1016/j.molcata.2016.02.022>
- [4] Chen Z, Yu X, Song Y (2016) Palladium nanoparticle supported on mesoporous polybenzimidazole as a heterogeneous catalyst for Suzuki cross-coupling reaction in aqueous media. *Ferroelectrics* 494:200–207. <https://doi.org/10.1080/00150193.2016.1134037>
- [5] Dong Y, Ju JJ, Li Y, Li WH, Chen YQ, Sun Q, Ma JP, Dong YB (2019) Nickel-metalated porous organic polymer for Suzuki–Miyaura cross-coupling reaction. *RSC Adv* 9:20266–20272. <https://doi.org/10.1039/c9ra03679b>
- [6] Kargar S, Elhamifar D (2020) Ionic liquid-containing polyethylene supported palladium: a green, highly efficient and stable catalyst for Suzuki reaction. *Mater Today Chem* 17:100318. <https://doi.org/10.1016/j.mtchem.2020.100318>
- [7] Chakraborty J, Nath I, Verpoort F (2019) Pd-nanoparticle decorated azobenzene based colloidal porous organic polymer for visible and natural sunlight induced Mott-Schottky junction mediated instantaneous Suzuki coupling. *Chem Eng J* 358:580–588. <https://doi.org/10.1016/j.cej.2018.09.037>
- [8] Ren XM, Kong SN, Shu QD, Shu MH (2016) Palladium nanoparticles supported on a porous organic polymer: an efficient catalyst for Suzuki–Miyaura and Sonogashira coupling reactions. *Chin J Chem* 34:373–380. <https://doi.org/10.1016/j.cej.2018.09.037>
- [9] Wang CA, Han YF, Li YW, Nie K, Cheng XL, Zhang JP (2016) Bipyridyl palladium embedded porous organic polymer as highly efficient and reusable heterogeneous catalyst for Suzuki–Miyaura coupling reaction. *Rsc Adv* 6:34866–34871. <https://doi.org/10.1039/c6ra03331h>
- [10] Wan YL, Song FX, Ye T, Li GX, Liu DF, Lei YZ (2019) Carbonylative Suzuki coupling and alkoxycarbonylation of aryl halides using palladium supported on phosphorus-doped porous organic polymer as an active and robust catalyst: carbonylative Suzuki coupling and alkoxycarbonylation of aryl halides. *Appl Organomet Chem* 33:e4714. <https://doi.org/10.1002/aoc.4714>
- [11] Song X, Li YX, Zhou L, Liu N, Wu ZQ (2022) Controlled synthesis of one-handed helical polymers carrying achiral organoiodine pendants for enantioselective synthesis of quaternary all-carbon stereogenic centers. *Macromolecules* 55:4441–4449. <https://doi.org/10.1021/acs.macromol.2c00810>
- [12] Liu N, Zhou L, Wu ZQ (2021) Alkyne-palladium(II)-catalyzed living polymerization of isocyanides: an exploration of diverse structures and functions. *Acc Chem Res* 54:3953–3967. <https://doi.org/10.1021/acs.accounts.1c00489>
- [13] Hou XH, Chen XJ, Gao X, Xu L, Zou H, Zhou L, Wu ZQ (2021) Synthesis of cyclic polyolefin: ring-opening metathesis polymerization by binuclear vanadium complexes†. *Chin J Chem* 39:1181–1187. <https://doi.org/10.1002/cjoc.202000636>
- [14] Zou H, Wu QL, Zhou L, Hou XH, Liu N, Wu ZQ (2021) Chiral recognition and resolution based on helical polymers. *Chin J Polym Sci* 39:1521–1527. <https://doi.org/10.1007/s10118-021-2615-y>
- [15] Wang C, Zou H, Liu N, Wu ZQ (2021) Recent advances in polyallenes: preparation, self-assembly, and stimuli-responsiveness. *Chem Asian J* 16:3864–3872. <https://doi.org/10.1002/asia.202101051>
- [16] Huang YB, Qiang W, Liang J, Wang X, Cao R (2016) Soluble metal-nanoparticle-decorated porous coordination polymers for the homogenization of heterogeneous catalysis. *J Am Chem Soc* 138:10104–10107. <https://doi.org/10.1021/jacs.6b06185>
- [17] Doherty S, Knight JG, Backhouse T, Abood E, Alshaiikh H, Fairlamb I, Bourne RA, Chamberlain TW, Stones R (2017) Highly efficient aqueous phase chemoselective hydrogenation of  $\alpha$ ,  $\beta$ -unsaturated aldehydes catalysed by phosphine-decorated polymer immobilized IL-stabilized PdNPs. *Green Chem* 19:1635–1641. <https://doi.org/10.1039/c6gc03528k>
- [18] Gholinejad M, Zareh F, Najera C (2018) Iron oxide modified with pyridyl-triazole ligand for stabilization of gold nanoparticles: an efficient heterogeneous catalyst for A 3 coupling reaction in water: a new gold catalyst introduced in A3 coupling reaction in water. *Appl Organomet Chem* 32:e4454. <https://doi.org/10.1002/aoc.4454>
- [19] Hajipour AR, Sadeghi AR, Khorsandi Z (2018) Pd nanoparticles immobilized on magnetic chitosan as a novel reusable catalyst for green Heck and Suzuki cross-coupling reaction: in water at room temperature. *Appl Organomet Chem* 32:e4112. <https://doi.org/10.1002/aoc.4112>
- [20] Li LY, Zhao HX, Wang JY, Wang RH (2014) Facile fabrication of ultrafine palladium nanoparticles with size- and location-control in click-based porous organic polymers. *ACS Nano* 8:5352–5364. <https://doi.org/10.1021/nn501853g>

- [21] Debruyne M, Speybroeck VV, Voort P, Stevens CV (2021) Porous organic polymers as metal free heterogeneous organocatalysts. *Green Chem* 23:7361–7434. <https://doi.org/10.1039/d1gc02319e>
- [22] Rashidi S, Kashefi MH, Kim KC, Samimi-Abianeh O (2019) Potentials of porous materials for energy management in heat exchangers-A comprehensive review. *Appl Energ* 243:206–232. <https://doi.org/10.1016/j.apenergy.2019.03.200>
- [23] Fast CD, Woods J, Lentchner J, Makal TA (2019) Stabilizing defects in metal-organic frameworks: pendant lewis basic sites as capping agents in UiO-66-type MOFs toward highly stable and defective porous materials. *Dalton T* 48:14696–14704. <https://doi.org/10.1039/c9dt03004b>
- [24] Song K, Jiang Y, Zou Z (2020) Effect of vesicle structure on catalytic activity of Suzuki–Miyaura cross-coupling reaction: impact of framework and morphology. *Chem Sel* 5:11438–11445. <https://doi.org/10.1002/slct.202003233>
- [25] Yang D, Hou YL, Zhuang Q, Liu P, Kong J (2019) Nitrogen-rich porous organic polyamines for stabilization of highly dispersed metal nanoparticles and catalytic application. *Macromol Rapid Comm* 40:1900100-1–1900100-8. <https://doi.org/10.1002/marc.201900100>
- [26] Lin H, Gao X, Yao H, Luo Q, Xiang B, Liu C, Ouyang Y, Zhou N, Xiang D (2021) Immobilization of a Pd(II)-containing N-heterocyclic carbene ligand on porous organic polymers: efficient and recyclable catalysts for Suzuki–Miyaura reactions. *Catal Sci Technol* 11:3676–3680. <https://doi.org/10.1039/d1cy00021g>
- [27] Tao R, Ma XR, Wei XL, Jin YH, Qiu L, Zhang W (2020) Porous organic polymer material supported palladium nanoparticles. *J Mater Chem A* 8:17360–17391. <https://doi.org/10.1039/d0ta05175f>
- [28] Modak A, Ghosh A, Mankar AR, Pandey A, Selvaraj M, Pant KK, Chowdhury B, Bhaumik A (2021) Cross-linked porous polymers as heterogeneous organocatalysts for task-specific applications in biomass transformations, CO<sub>2</sub> fixation, and asymmetric reactions. *ACS Sustain Chem Eng* 9:12431–12460. <https://doi.org/10.1021/acssuschemeng.1c01537>
- [29] Xu XH, Li YX, Zhou L, Liu N, Wu ZQ (2022) Precise fabrication of porous polymer frameworks using rigid polyisocyanides as building blocks: from structural regulation to efficient iodine capture†. *Chem Sci* 13:1111–1118. <https://doi.org/10.1039/d1sc05361b>
- [30] Wu K, Guo J (2015) Controllable synthesis of multi-scale conjugated microporous polymers. *Acta Chim Sinica* 73:480–486. <https://doi.org/10.6023/A15020138>
- [31] Tan LX, Tan B (2017) Hypercrosslinked porous polymer materials: design, synthesis, and applications. *Chem Soc Rev* 46:3481–3481. <https://doi.org/10.1039/c7cs90027a>
- [32] Lan S, Yang X, Shi KJ, Fan R, Ma D (2019) Pillarquinone-based porous polymer for a highly-efficient heterogeneous organometallic catalysis. *Chem Cat Chem* 11:2864–2869. <https://doi.org/10.1002/cctc.201900516>
- [33] Wang CA, Li YW, Hou XM, Han YF, Nie K, Zhang JP (2016) N-heterocyclic carbene-based microporous organic polymer supported palladium catalyst for Carbon–Carbon coupling reaction. *Chem Sel* 1:1371–1376. <https://doi.org/10.1002/slct.201600174>
- [34] Zhang Y, Zhang L, Zhang XL, Yang DD, Du C, Wan L, Au C, Chen J, Xie MJ (2020) Pyridine-based hypercrosslinked polymers as support materials for palladium photocatalysts and their application in Suzuki–Miyaura coupling reactions. *New J Chem* 44:15202–15208. <https://doi.org/10.1039/d0nj01675f>
- [35] Gao PW, Xiao YM, Dong ZH, Pan HG, Wang WT (2020) Facile synthesis of palladium nanoparticles supported on urea-based porous organic polymers and its catalytic properties in Suzuki–Miyaura coupling. *J Saudi Chem Soc* 24:282–287. <https://doi.org/10.1016/j.jscs.2019.11.002>
- [36] Lei YZ, Lan GS, Zhu DJ, Wang RS, Zhou XY, Li GX (2018) Urea-based amphiphilic porous organic polymer-supported palladium as a reusable catalyst for Suzuki–Miyaura coupling and hydroxycarbonylation reactions in water. *Appl Organomet Chem* 32:e4421. <https://doi.org/10.1002/aoc.4421>
- [37] Ding XS, Han BH (2015) Metallophthalocyanine-based conjugated microporous polymers as highly efficient photosensitizers for singlet oxygen generation. *Angew Chem Int Edit* 54:6536–6539. <https://doi.org/10.1002/anie.201501732>
- [38] Liu XM, Xu YH, Jiang DL (2012) Conjugated microporous polymers as molecular sensing devices: microporous architecture enables rapid response and enhances sensitivity in fluorescence-on and fluorescence-off sensing. *J Am Chem Soc* 134:8738–8741. <https://doi.org/10.1021/ja303448r>
- [39] Liras M, Iglesias M, Sánchez F (2016) Conjugated microporous polymers incorporating BODIPY moieties as light-emitting materials and recyclable visible-light photocatalysts. *Macromolecules* 49:1666–1673. <https://doi.org/10.1021/acs.macromol.5b02511>
- [40] Su C, Tandiana R, Tian B, Sengupta A, Tang W, Su J, Loh K (2016) Visible-light photocatalysis of aerobic oxidation reactions using carbazolic conjugated microporous polymers. *ACS Catal* 6:3594–3599. <https://doi.org/10.1021/acscatal.6b00443>
- [41] Dey SK, Dietrich D, Wegner S (2018) Palladium nanoparticle-immobilized porous polyurethane material for quick

- and efficient heterogeneous catalysis of Suzuki–Miyaura cross-coupling reaction at room temperature. *Chem Sel* 3:1365–1370. <https://doi.org/10.1002/slct.201702083>
- [42] Qing CG, Liu QL, Zhou WT, Hui GH, Guo Y (2017) Palladium nanoparticles supported on a carbazole functionalized mesoporous organic polymer: synthesis and their application as efficient catalysts for the Suzuki–Miyaura cross coupling reaction. *Polym Chem-UK* 8:1488–1494. <https://doi.org/10.1039/c6py01784c>
- [43] Arab P, Verlander A, El-Kaderi HM (2015) Synthesis of a highly porous bis (imino) pyridine-linked polymer and its postsynthetic modification with inorganic fluorinated ions for selective CO<sub>2</sub> capture. *J Phys Chem C* 119:8174–8182. <https://doi.org/10.1021/acs.jpcc.5b00690>
- [44] Modak A, Pramanik M, Inagaki S, Bhaumik A (2014) A triazine functionalized porous organic polymer: excellent CO<sub>2</sub> storage material and support for designing Pd nanocatalyst for C–C cross-coupling reactions. *J Mater Chem A* 2:11642–11650. <https://doi.org/10.1039/c4ta02150a>
- [45] Bhunia A, Vasylyeva V, Janiak C (2013) From a supramolecular tetranitrile to a porous covalent triazine-based framework with high gas uptake capacities. *Chem Commun* 49:3961–3963. <https://doi.org/10.1039/c3cc41382a>
- [46] Ju PY, Wu SJ, Su Q, Li XD, Liu ZQ, Li GH, Wu QL (2019) Salen-porphyrin-based conjugated microporous polymer supported Pd nanoparticles: highly efficient heterogeneous catalysts for aqueous C–C coupling reactions. *J Mater Chem A* 7:2660–2666. <https://doi.org/10.1039/c8ta11330k>
- [47] Liao YZ, Cheng ZH, Zuo WW, Thomas A, Faul C (2017) Nitrogen-rich conjugated microporous polymers: facile synthesis, efficient gas storage and heterogeneous catalysis. *Acs Appl Mater Interfaces* 9:38390–38400. <https://doi.org/10.1021/acsmi.7b09553>
- [48] Lee J, Chang JY (2018) Synthesis of a palladium acetylide-based tubular microporous polymer monolith via a self-template approach: a potential precursor of supported palladium nanoparticles for heterogeneous catalysis. *Rsc Adv* 8:25277–25282. <https://doi.org/10.1039/c8ra03275k>
- [49] Chen J, Zhang J, Zhang Y, Xie MJ, Li T (2020) Nanoporous phenanthroline polymer locked Pd as highly efficient catalyst for Suzuki–Miyaura coupling reaction at room temperature. *Appl Organomet Chem* 34:e5310. <https://doi.org/10.1002/aoc.5310>
- [50] Xu L, Cui J, Gao S, Wang JJ, Liu J, Jia HG, Zhang ZF, Miao FJ, Zang Y (2022) Synthesis of Pd-stabilized chiral conjugated microporous polymer composites as high efficiency heterogeneous asymmetric Henry reaction catalysts. *Microporous Mesoporous Mat* 341:112075. <https://doi.org/10.1016/j.micromeso.2022.112075>
- [51] Ratnam A, Bala M, Kumar R, Singh UP, Ghosh K (2017) Design and syntheses of a new family of palladium complexes derived from tridentate ligands and their application as catalysts for Suzuki–Miyaura cross-coupling reactions. *J Organomet Chem* 856:41–49. <https://doi.org/10.1016/j.jorganchem.2017.12.017>

**Publisher's Note** Springer Nature remains neutral with regard to jurisdictional claims in published maps and institutional affiliations.

Springer Nature or its licensor (e.g. a society or other partner) holds exclusive rights to this article under a publishing agreement with the author(s) or other rightsholder(s); author self-archiving of the accepted manuscript version of this article is solely governed by the terms of such publishing agreement and applicable law.